ARTICLE

The Anatomical Record
Advances in Integrative Anatomy and Evolutionary Biology

WILEY

Ongoing tissue changes in an experimentally mummified human leg

Irina Morozova[1] | Lena M. Öhrström[1] ⓘ | Patrick Eppenberger[1] |
Beata Bode-Lesniewska[2] | Dominic Gascho[3] | Cordula Haas[3] |
Gülfirde Akgül[1] | Judith Neukamm[1,4,5] | Kim A. Röthlin[6] | Alexander Imhof[7] |
Natallia Shved[1] | Christina Papageorgopoulou[8] | Frank J. Rühli[1]

[1]Institute of Evolutionary Medicine, Faculty of Medicine, University of Zurich, Zurich, Switzerland

[2]Institute of Pathology and Molecular Pathology, University Hospital Zurich, Zurich, Switzerland

[3]Zurich Institute of Forensic Medicine, University of Zurich, Zurich, Switzerland

[4]Institute for Archaeological Sciences, University of Tübingen, Tübingen, Germany

[5]Center for Bioinformatics Tübingen, University of Tübingen, Tübingen, Germany

[6]Institute of Medical Microbiology, Faculty of Medicine, University of Zurich, Zurich, Switzerland

[7]SRO AG, Spital Langenthal, Department of Internal Medicine, Langenthal, Switzerland

[8]Laboratory of Physical Anthropology, Department of History and Ethnology, Democritus University of Thrace, Komotini, Greece

Correspondence
Lena M. Öhrström, Institute for Evolutionary Medicine, Faculty of Medicine, University of Zurich, Winterthurerstr. 190, 8057 Zurich, Switzerland.
Email: lena.ohrstrom@iem.uzh.ch

Abstract

Artificial mummification has been used since antiquity and is best known from ancient Egypt. Despite ancient Egyptian mummies being studied for several decades, the mummification techniques of that time are not well understood. Modern mummification experiments involving animal and human tissues have contributed additional insights relevant to a broad field of research. In the current study, we present follow-up results of an experiment on artificial mummification, which began in 2009. A human leg was artificially mummified and monitored for almost a year with histological, molecular, and radiological techniques. Since then, it has remained in a dry, natron salt blend for 9 years. The current analyses show further progression of dehydration and tissue alterations, as well as DNA degradation, suggesting an ongoing process. Our results add new insights into the mechanisms of tissue mummification. Taking into account that the process is still ongoing, further research is required, including a re-evaluation of the human leg in the future.

KEYWORDS
forensic, histology, imaging, molecular investigations, mummified

Irina Morozova and Lena M. Öhrström contributed equally to this study.

1 | INTRODUCTION

The scientific study of mummies is of broad interest with impact in various research fields including archeology, physical anthropology, paleogenetics, medicine, and forensics. Mummies are not only fascinating historical and cultural artifacts but also a valuable source for the study of human evolution and disease (Aufderheide, 2000; Thompson et al., 2013).

Natural mummification can occur under particular environmental conditions, such as in deserts, salty areas, crypts, or moors. Artificial or anthropogenic mummies are known from several cultures and periods, the best known of which are those of ancient Egypt. The ancient Egyptians treated the bodies of the dead, convinced of their need in the afterlife. Despite ancient mummies having been studied for several decades, the mummification techniques of this period are not well understood. The only written sources date back to Herodotus (c. 484 BC– c. 425 BC) (Herodot, 2000) and Diodorus Siculus (c. 90–c. 30 BC) (Diodorus, 1985) and were written at the end of the Egyptian kingdom. In addition, much of our knowledge about mummification comes from tomb inscriptions and preserved papyri that deal with ritual aspects (Ikram & Dodson, 1998). Still today, there is a broad interest, also in forensics, to gain more knowledge about those techniques. Several experimental mummification studies have been performed with animal models (Garner, 1979; Notman & Aufderheide, 1992; Oh & Shin, 2014), but only a few human mummification studies have been completed so far. A whole body was successfully experimentally mummified by Brier and Wade (1997); however, no continuous radiological, histological, or biochemical analyses have been undertaken during the mummification process.

In 2009, we started an experiment on artificial mummification of a human leg (Panzer et al., 2013; Papageorgopoulou, Shved, Wanek, & Rühli, 2015; Shved et al., 2014). The experiment aimed to track tissue alterations during the mummification process in real-time. The focus of the experiment was on the desiccation process in a salt-rich environment, either under natural conditions or in anthropogenic mummification, as exemplified in ancient Egypt. Macroscopic, molecular, histological, and radiological alterations were assessed. At the end of the first 322 days of the experiment, a very advanced state of mummification was found. At the molecular level, continuous degradation of DNA was observed, histologically, the tissues underwent continuous degradation over time, and radiologically, progressive dehydration accompanied by varying tissue alterations was seen. Although certain regions did not fully desiccate, no macroscopic tissue destruction or decomposition was noticed.

In this article, we present the results of a follow-up analysis 9 years after the beginning of the original experiment. The leg has remained preserved in a dry, natron salt blend up until now. To identify any further tissue alterations, we have now re-examined the leg using molecular, histological, and radiological methods.

# 2 | MATERIALS AND METHODS

2.1 | Materials

In the previously performed experiment in May 2009, a left lower leg (with intra-vitam body declaration and ethics committee approval) was amputated 24 hr postmortem and artificially mummified. The desiccation process was simulated according to the technique reportedly used in ancient Egypt. Seventy kilograms of a blend of natron salts, a naturally occurring mixture of sodium chloride, sodium sulfate, sodium carbonate, and sodium bicarbonate, were used. In ancient Egypt, natural natron used for the mummification process was mostly collected from the Wadi Natrun desert in present-day northern Egypt. Chemically pure components were powdered and dehydrated at 100°C, then mixed according to the formula outlined in Brier and Wade: 54% NaCl, 16% Na_2SO_4, 18% Na_2CO_3, and 12% $NaHCO_3$ (Brier & Wade, 1997). Radiological, histological, and molecular analyses were performed repeatedly, documenting the mummification process (Panzer et al., 2013; Papageorgopoulou et al., 2015; Shved et al., 2014). The original experiment was closely monitored for 322 days, after which the leg was mostly mummified and showed a leathery appearance. However, particular areas, such as the thigh and foot, did not completely dehydrate (Figure 1A,B). This circumstance could be explained by the climate (i.e., cooler environment, also not as arid as in Egypt) and some lack of ventilation. Since then, the leg has been kept under stable conditions (including humidity and temperature), covered with a blend of natron salts, in a laboratory at the Institute of Evolutionary Medicine.

In the current study, similar analyses have been conducted between 8 and 9 years after the end of the original 322-day experiment.

2.2 | Methods

2.2.1 | Radiological analyses

Radiological analyses were performed in 2017 at the Forensic Institute of the University of Zurich, using a clinical CT Scanner: Somatom Definition Flash (Siemens Healthcare, Forchheim, Germany) as well as a clinical
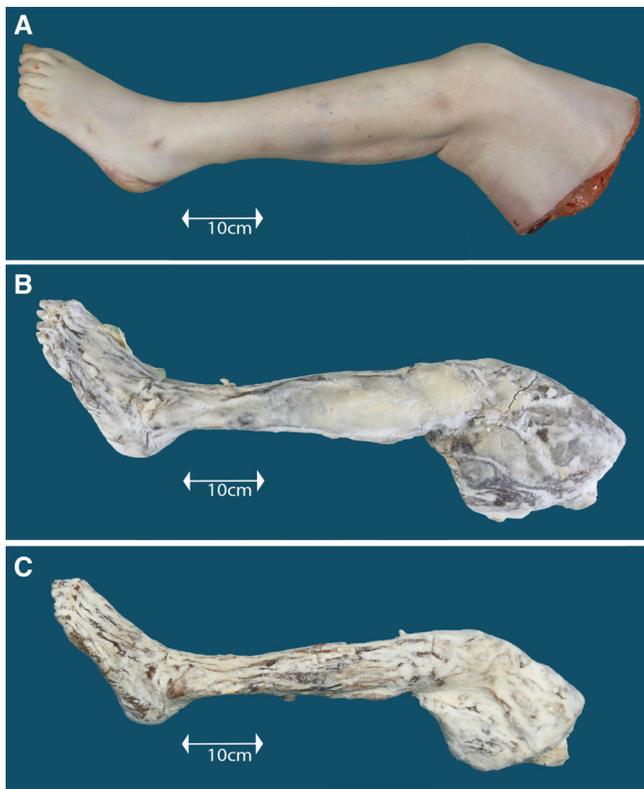
FIGURE 1 Photo of the human lower leg, (A) Day 0 (co Heinz Sonderegger); (B) Day 208 (co Heinz Sonderegger); (C) now, after 9 years (co Lena Öhrström)

magnetic resonance imaging (MRI) scanner: 3 Tesla Achieva (Philipp Healthcare, Best, The Netherlands) using an XL Torso coil. The CT scan parameters were as follows: 120 kVp (tube voltage) and 860 mA s (tube current) reconstructed with a slice thickness of 0.6 mm (increment: 0.4 mm) in an adjusted field of view. The MRI examination included T1-weighted sequences (TR: 636.2 and TE: 6.9) and T2-weighted sequences (TR: 4141.8 and TE: 60.0) with a slice thickness of 5 mm. Fifty slices in transversal orientation were acquired in both weightings for the distal part and the proximal part of the leg. Inversion recovery sequences were not performed for comparison with Panzer et al., since their selected inversion time (TI) was not indicated. Additionally, ultra-short echo (UTE) sequences using vendor-specific software patches were also deemed unnecessary with sufficient signal contrast in the T1-weighted and T2-weighted images. Furthermore, Panzer et al. did not evaluate their UTE sequences.

The resulting images were qualitatively analyzed, and the main tissue-types, that is, skin, muscle tissue, compact bone, and cartilage, were quantitatively evaluated as was performed during the original study (Panzer et al., 2013). Dedicated software (OsiriX–MD 64 bit, version 8.0.1; Pixmeo, Switzerland) was used for image evaluation. Hounsfield units (HU) for CT and signal intensity (SI) for

MR were measured within defined regions of interest (ROIs) by two individual readers (LO and PE), both physicians with several years of experience in paleoradiological research. For each tissue-category, three measurements were taken by each reader; mean values were then calculated for every three corresponding measurements. Following the original study, all soft tissue structures—apart from cartilage—were analyzed at the level of the middle third of the lower leg. The cartilage was analyzed at the level of the patella (Figure 2). Care was taken to reproduce ROI size and placement as close to the original publication as possible. Where possible, results were then compared to the findings of the original study.

2.2.2 | Histological analyses

Two small samples for histological analyses were taken at the distal third of the medial lower leg, punch biopsy (internal No. 100), as well as in the mid of the lower leg, medial (internal No. 104). Histological analyses were performed at the Institute of Pathology and Molecular Pathology of the University Hospital, Zurich, Switzerland. The samples were rehydrated, fixed by immersion in buffered 4% formalin, and embedded in paraffin. Two micrometer thick sections were cut and stained with hematoxylin and eosin (H&E) and Elastica-van-Gieson according to standard routine procedures.

2.2.3 | Molecular analyses

The samples from the previous stages of the experiment were kept at −20°C since the beginning of the experiment until the present time. The new samples (muscle and skin) were taken in October 2017 from the mid-calf sampling area as previously described (Shved et al., 2014).

DNA extraction. DNA was extracted from muscle and skin samples from the following time points: Stage 0 (beginning of the experiment; M0 and S0, respectively), Stage I (end of the first stage of the experiment; MI, SI), and Stage II (current status, 8 years after the beginning of the experiment, MII, SII). Therefore, DNA from seven samples in total (six experimental plus a negative control) was extracted using the same method as described in Shved et al. (2014) using QIAamp DNA Mini Kit (Qiagen) following the manufacturer's protocol. About 23–31 mg of tissue was used for extraction. In the end, DNA was dissolved in 60-μl of elution buffer. DNA quantity was assessed using a Qubit fluorometer (Thermo Fisher Scientific).

DNA fragmentation analysis. DNA fragmentation in samples from Stage II was assessed, first, via gel-electrophoresis (1 μl of DNA extract in 0.8% agarose gel),
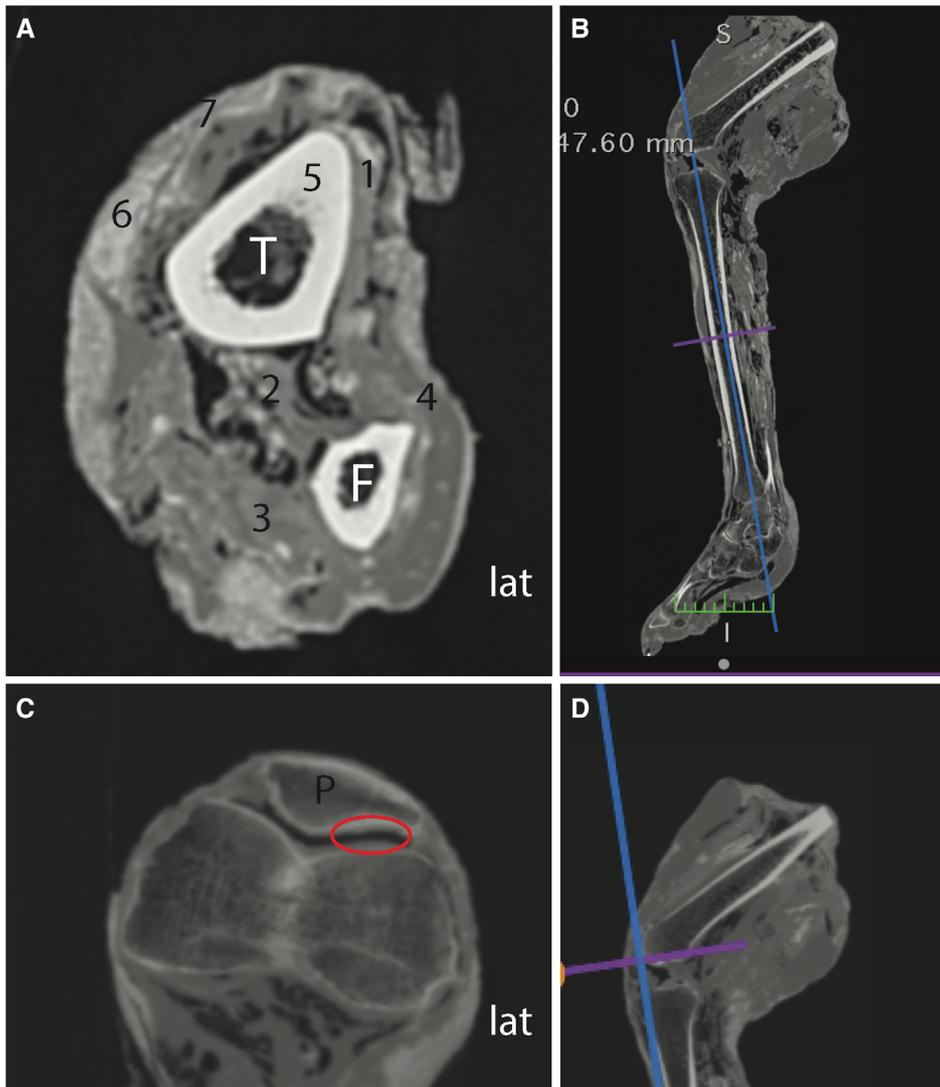
FIGURE 2 Location of the radiology measurements, illustrated on CT. (A) axial slice at mid-lower leg; (1) Tibialis anterior muscle, (2) Tibialis posterior muscle, (3) Soleus muscle, (4) Peroneus muscle, (5) Compact bone, (6) Subcutis, (7) Cutis; T: tibia, F: fibula. (B) Slice location (violet line). (C) Axial slice at the knee level, for cartilage measurements (red circle), P: patella. (D) Slice location (violet line)

second, using Agilent 2200 TapeStation System (with High Sensitivity D1000 Screen Tapes).

Autosomal Short Tandem Repeats (STR) analysis. STR analysis was performed at the Zurich Institute of Forensic Medicine, University of Zurich. DNA extracts from Stage II samples were amplified using the AmpFLSTR™ NGM SElect™ PCR Amplification Kit (Thermo Fisher) according to the manufacturer's instructions. Thirty amplification cycles were run. PCR products were separated and detected with a Genetic Analyzer 3130xl. Amplicons of the STR loci were up to 450 bp in length. Raw data were analyzed with the Genemapper ID-X Software Version 1.4 (Thermo Fisher). A threshold of 50 RFUs was used for peak detection.

Next generation sequencing analysis. To assess the changing of DNA damage profile during the 8 years, the skin and muscle samples from Stage 0, Stage I, and Stage II were analyzed using high-throughput sequencing. The library preparation was performed according to the

TABLE 1 Concentration (µg/ml) of DNA extracted from muscle and skin samples during three stages of the mummification experiment

	Stage 0	Stage I	Stage II
Muscle	89.7	4.51	0.359
Skin	89.9	76.2	88.6

protocols for ancient DNA (Kircher, Sawyer, & Meyer, 2012; Meyer & Kircher, 2010). Since the DNA concentrations in samples M0, S0, SI, and SII were relatively high in comparison to other samples (Table 1), the 1:10 dilutions were used to make libraries from these samples; for other samples, non-diluted DNA was used. Before the library preparation, DNA was sheared by ultrasound using a Covaris sonicator according to the manufacturer protocol. The resulting fragments were about 300 bp in length. The sequencing was performed at the Functional Genomic

Centre Zurich, Switzerland, on Illumina HighSeq4000 with $2 \times 150 + 8 + 8$ cycles. The sequencing data were analyzed using EAGER v.1.92.33 software (Peltzer et al., 2016).

2.2.4 | Bacteriology

Standard bacteriological analyses of one muscle sample (middle-lower leg, fronto-laterally; punch biopsy) was performed at the Hospital Langenthal, Switzerland.

2.2.5 | pH measurements and temperature

Measurement of pH was done with indicator strips (universal indicator 0-14; Merck, kGaA, Darmstadt, Germany) on the molecular samples (muscle and skin), which were taken from the mid-calf sampling area. The temperature was measured with an electronic digital thermometer "MULTI," Huberlab, Switzerland. Circumstance conditions were stable with an external temperature of 22°C and a relative air humidity of 56%.

3 | RESULTS

Macroscopically, the leg has changed in size; however, the appearance in terms of color and consistency did not significantly change since the end of the first phase of the experiment after 322 days. While most parts are now fully mummified, the thigh and foot in particular still feature certain areas that are not entirely dehydrated. However, no signs of decomposition of the sample were noted in any area (Figure 1). Overall, the leg lost a substantial amount of weight over the past 9 years. While the leg initially weighed 6 kg, and the weight dropped to 3.5 kg after the first 208 days of the experiment; currently, the leg weighs 2.4 kg. Thus, the weight of the leg dropped to 58% of its initial value by the end of the first phase of the experiment and has since decreased further by 31.5%, now only weighing 40% of its initial weight.

3.1 | pH measurements

The pH values did not change significantly over the past 9 years. The current measurement indicated an alkaline pH of 9 for the muscle sample and a slightly higher pH of 10 for the skin sample. At the beginning of the experiment, the pH values of the fresh tissues were all in the neutral range of 6–7, and then, with some initial fluctuations, increased steadily during mummification in the alkaline natron salt blend throughout the first phase of the experiment (final values: pH of 9 for muscle and pH of 10 for skin).

3.2 | Radiology

Overall, the radiological examinations show further tissue shrinkage (Figure 3). Interpretation of anatomical structures is mostly complicated by additional air inclusions and further tissue contractions. Particularly, the differentiation of myofascial structures presented some difficulties. In addition, several hyper-dense areas (~700 HU) of unclear origin, measuring up to max 10×20 mm^2, were identified in muscles and soft tissues on the CT scans. The sampling areas, that is, the places where earlier samples had been regularly taken, also altered the surface structure over time in certain cases. On MRI scans, distinguishing between different tissues, especially between different muscles or muscle groups, was even more difficult.

3.2.1 | CT measurements

In the following, the HU values from our ROI measurements were compared with the HU values originally published by Panzer et al.

Cutis: Mean HU is 639 (606 and 672 [interpreter 1 and interpreter 2, respectively]). The value decreased further from the end value of 737 on Day 60, which is congruent with the trend seen before.

Subcutis: Mean HU value is −52 (−56 and −48 [interpreter 1 and interpreter 2, respectively]). The value increased further from −78 on Day 60, which is also similar to the trend seen before.

Cartilage: Mean HU value is 377 (interpreter 1: 272; interpreter 2: 483). The value decreased from the end value of 340 on Day 60, which is counter to the trend seen before. However, significant interobserver differences were noted.

Compact bone: Mean HU value is 1,630 (interpreter 1: 1567; interpreter 2: 1693). The value decreased from the final value of 1,760, which is counter to the trend seen before.

Muscles: The mean HU values vary widely, ranging from 95 to 140. The mean value of all measured muscles is 132 and 199 (interpreter 1 and interpreter 2, respectively). The value decreased from the final mean value of 223, which is clearly counter to the trend seen before.

3.2.2 | MRI measurements

For a qualitative comparison, we repeated the approach of Panzer et al., according to which, over
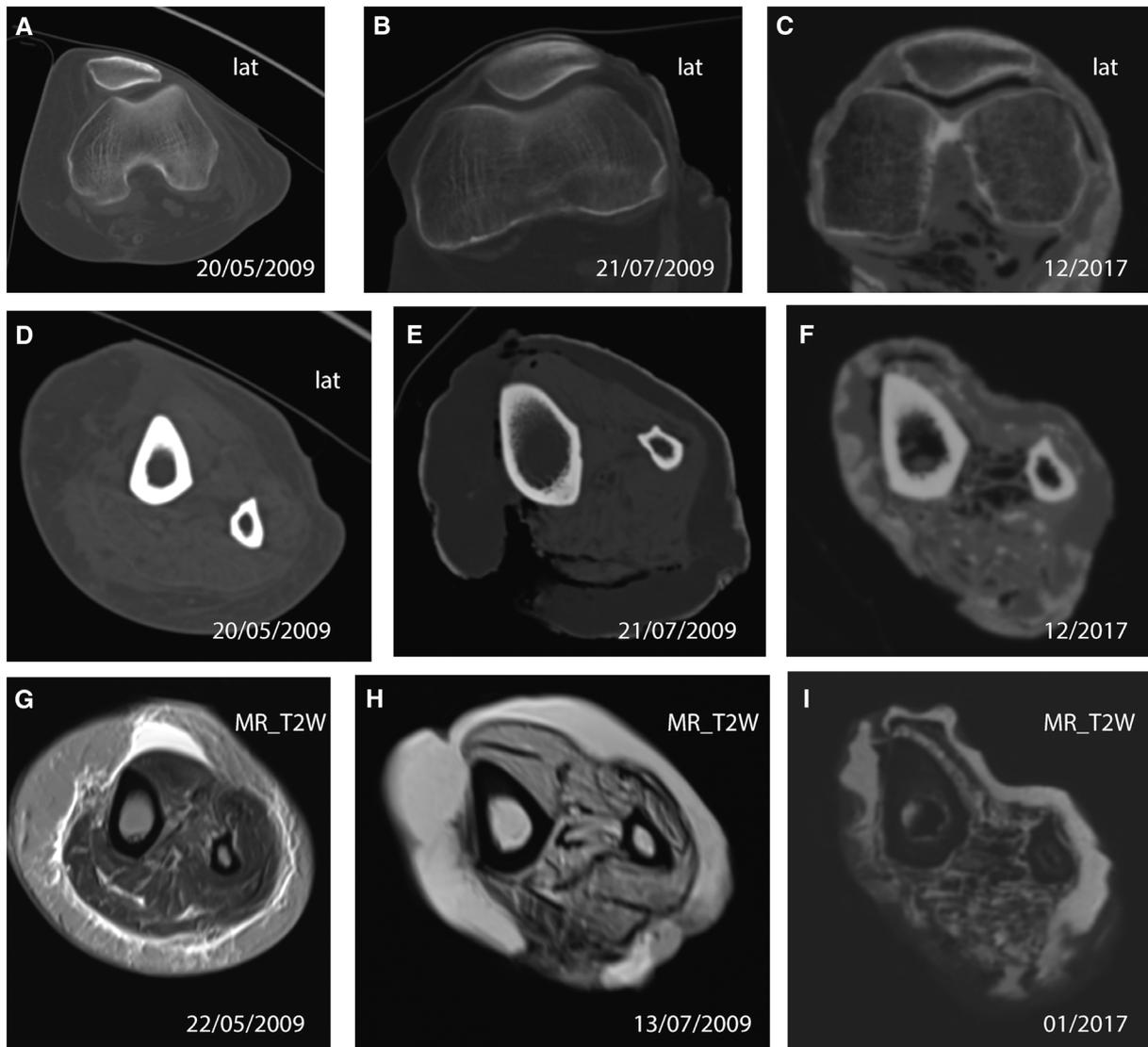
FIGURE 3 Radiological alterations over time at selected dates (start of experiment—left column; end-stage of first experiment—middle column; and after 8–9 years—right column. The alterations are presented on CT (axial view) at the level of the patella (A–C) and the mid-lower leg (D–F) as well as on T2-weighted MRI (axial view) at the corresponding mid-lower leg (G–I). Note the augmentation of density in the cutis on CT. On MRI, the tissue differentiation becomes more and more vague

the course of the experiment, signal intensities of different anatomical structures were measured across several MRI scans. The SI measurements differ widely across tissue as well as between observers. However, since SI values in standard T1- or T2-weighted MRI constitute qualitative values, they cannot be reliably compared between different acquisitions (Bergeest & Jäger, 2008). Therefore, only a qualitative assessment could be conducted.

Tissues are still identifiable while being further shrunken and show more air inclusion. However, the exact identification of various muscles is not guaranteed. In conclusion, the MRIs are comparable to other examples of artificial and natural mummifications.

3.3 | Histology

The microscopical appearance of the tissue samples after 9 years is quite similar to the findings at the end of the previous stage of the experiment, on Day 208 (Papageorgopoulou et al., 2015), suggesting constant preservation of the histological details by the mummification process during this period. The fibers of the skeletal muscles are well preserved, even after 9 years (Figure 4A,B). The nuclei cannot be seen; however, the striation of the skeletal muscle cytoplasm can still be identified. The supporting soft tissue consists of necrotic adipocytes, collagen, and blood vessels. The microscopical appearance of the skin after 9 years reflects the changes described at Day 208 of mummification (Figure 4C,D). The
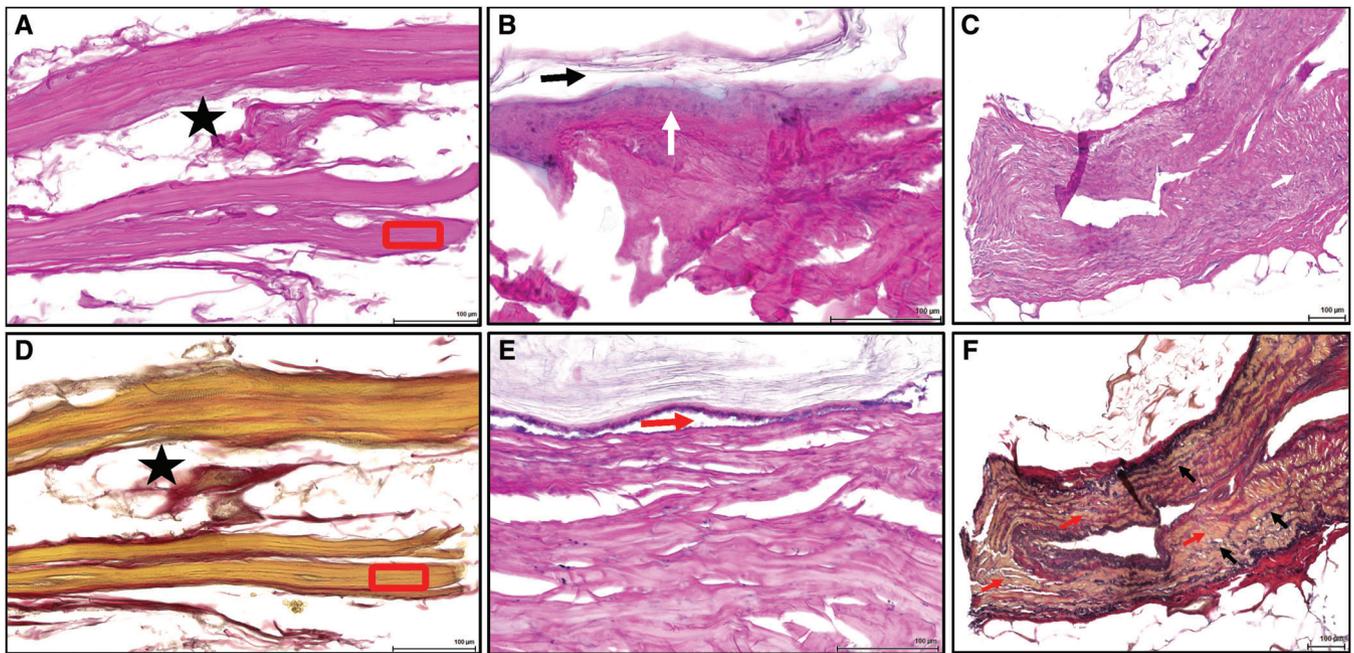
FIGURE 4 Histological analyses. Skeletal muscle in (A) H&E and (B) Elastica-van-Gieson staining. The muscle fibers are well preserved; however, no nuclei can be seen. The stratification of the cytoplasm is well visible (red rectangle). The supporting soft tissue (filled stars) consists of small blood vessels, necrotic fatty tissue, and collagen. (Original magnification 400×). Skin samples in the H&E staining (c/d) demonstrate the variable quality of the epidermis with some areas showing better preservation of the squamous stratification and intact basal layers seated on the basal membrane (white arrow) (C), while hardly recognizable stratification in others (D). There are various areas of epidermal detachment, either in the stratum corneum (black arrow in panel c) or in basal layers (red arrow in panel d). (Original magnification 400×). A well-preserved vein in (E) H&E and (F) Elastica-van-Gieson (EvG) stains. In the H&E stain, some nuclei of the smooth muscle cells in the tunica media of the vessel wall can be seen (white arrows). The structure of the vessel wall is well recognizable in the EvG stain (f) including smooth muscle (red arrow) and elastic fibers (black arrow). (Original magnification 400×)

epidermis shows variable preservation of the stratification and variable planes of detachment, either within the stratum corneum or within deeper epidermal layers. Hardly any nuclear details, of both epidermis or papillary dermis can be observed. Interestingly, the structure of some larger blood vessels (vein in Figure 4E,F) is remarkably well preserved, allowing for the identification of the vascular wall layers and showing the staining of the nuclei.

3.4 | Molecular analyses

3.4.1 | DNA concentration

The concentration of DNA extracted from samples from three different time points (Stages 0, I, and II) demonstrated different patterns for skin and muscle tissues. For skin samples, after 8 years of mummification DNA concentration stayed unchanged (Table 1). At the same time, there is a significant decrease in DNA quantity in muscle samples: starting from the same concentration as for the skin sample at Stage 0 (89.9 and 89.7 μg/ml, see Table 1), the DNA quantity decreased to 5% after nearly 1 year of mummification and decreased to 0.4% during the next

7 years (Table 1). This confirms the previous observation of Shved et al. (2014) about more intensive DNA damage in muscle tissues compared to skin.

3.4.2 | DNA fragmentation

Gel electrophoresis analysis shows a strong DNA smearing at Stage II, the pattern that was previously observed at the end of the first stage of the experiment (Shved et al., 2014). TapeStation analysis revealed peaks of fragment sizes of about 1,500–2,000 bp (taking into account the resolution of the assay) (Figure 5). Therefore, the average fragment lengths decreased from 8,000 bp for skin and 2,000–4,000 bp for muscle (Shved et al., 2014) to 1,500–2,000 bp in both tissues (Figure 5), although the longer fragments still can be observed, but in much smaller amounts (Figure 5).

It is worth noting that muscle DNA degraded to a greater degree than skin DNA. This is seen on the gel electrophorogram where muscle DNA is literally invisible (Figure 5). It was previously observed that DNA fragmentation began earlier in muscle samples (Shved et al., 2014). This trend continued, as muscle DNA degraded more rapidly.
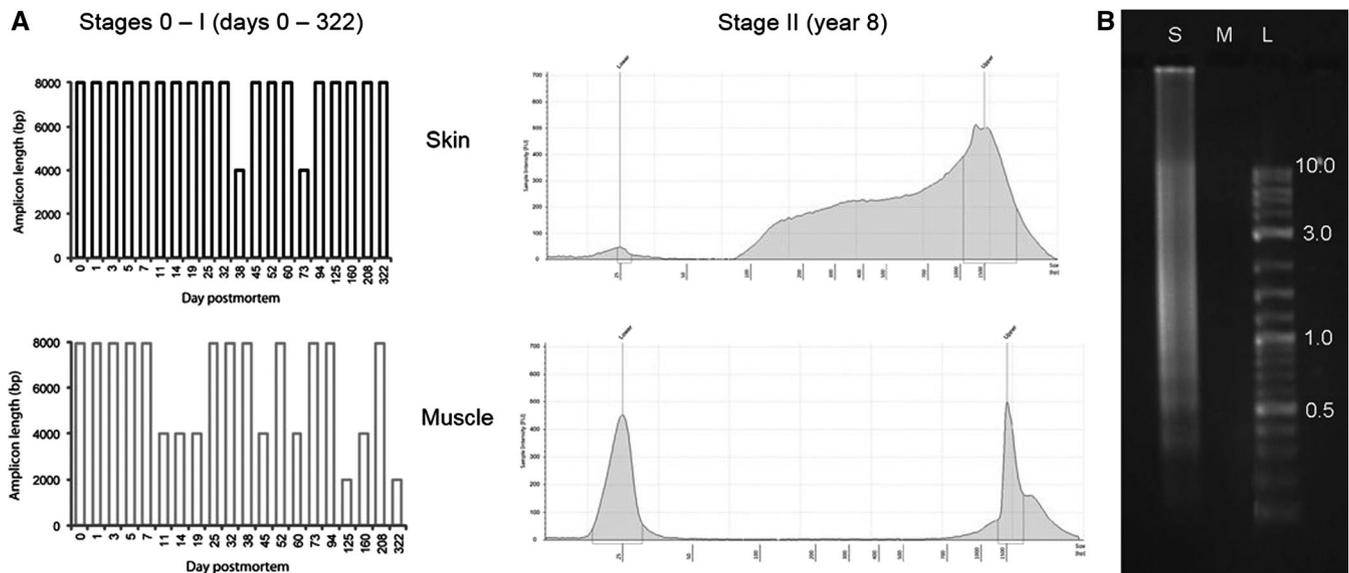
FIGURE 5 Analysis of DNA fragmentation at three main stages of the experiment. (A) PCR amplification analysis at Stages 0–I (Shved et al., 2014) and TapeStation analysis at Stage II; (B) Gel electrophoresis of genomic DNA at Stage II (M, muscle; S, skin; L, ladder (kB)

TABLE 2 Results of STR analysis

Marker	Muscle			Skin			Size allele 1	Size allele 2
	Stage 0	Stage I	Stage II	Stage 0	Stage I	Stage II		
vWA	16	16	16	16	16	16		171.5
D16S539	11, 12	11, 12	11, 12	11, 12	11, 12	11, 12	251.5	255.4
D2S1338	17, 25	17, 25	17, 25	17, 25	17, 25	17, 25	295.8	328.2
AMEL	X	X	X	X	X	X		98.6
D8S1179	13	13	13	13	13	13		142.5
D21S11	30, 31	30, 31	30, 31	30, 31	30, 31	30, 31	207.1	211.0
D18S51	15	15	15	15	15	15		293.2
D19S433	13, 14	13, 14	13, 14	13, 14	13, 14	13, 14	141.2	145.2
TH01	7	7	7	7	7	7		191.1
FGA	24, 25	24, 25	24, 25	24, 25	24, 25	24, 25	259.0	262.8
D3S1358	15, 18	15, 18	15, 18	15, 18	15, 18	15, 18	145.4	157.6

It is clear that the process of DNA degradation continues in skin: on the TapeStation electrophorogram, a long smear is visible, which demonstrates that DNA fragments with lengths up to 100 bp are present in the extract.

3.4.3 | STR analysis

STR analysis demonstrated no allelic dropout of STR markers up to 350 bp (Table 2), which is expected, given the results of the fragmentation assessment. The STR profiles of the samples from the first two stages of the experiment and the current stage are identical, confirming the absence of contamination during the present round of sampling and consequent molecular analysis.

3.4.4 | NGS analysis–DNA damage

Six DNA samples analyzed by next generation sequencing (NGS) (skin and muscle taken on Stage 0, Stage I, and Stage II) demonstrated the same whole-genome coverage (Supplementary Table 1).

DNA damage profiles for skin and muscle samples showed different patterns. Both groups demonstrated a tendency of increasing C > T changes at the ends of DNA fragments with time (Figure 6), which is a distinctive criteria

FIGURE 6 Frequencies of 5′C > T changes in NGS reads
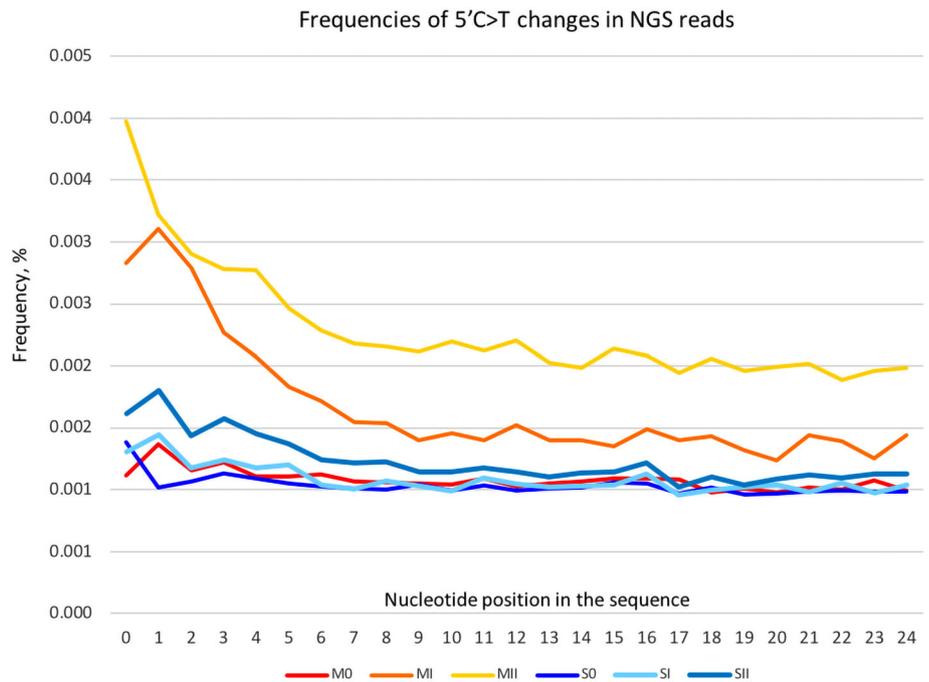
for characterizing ancient DNA (Gilbert et al., 2003; Hofreiter, Jaenicke, Serre, von Haeseler, & Paabo, 2001). However, for muscle samples, this tendency is more pronounced: the average frequency of C > T changes in the last seven nucleotides increased only 1.1× between Stage 0 and Stage I in the skin samples, while for the muscle samples, the misincorporation frequency increased nearly 2× (Supplementary Table 2). This process is still ongoing: the number of C > T changes at the ends of DNA fragments increased 1.4× in skin samples and 2.5× in muscle samples during the following 8 years of mummification (Supplementary Table 2).

It should be noticed that these numbers could be underestimated. C > T misincorporations occur more often in single-stranded overhangs arising as the results of DNA degradation postmortem (Gilbert et al., 2003; Hofreiter et al., 2001). In our case, as it was shown above, the average length of DNA fragments was about 1,500–2,000 bp. To prepare the DNA fragments for high-throughput sequencing, DNA was sheared artificially. Therefore, not only were the DNA ends resulting in natural DNA degradation analyzed but also the ends derived during the sonication and therefore do not possess DNA overhangs. Nevertheless, based on the observed tendency, one can expect further DNA fragmentation and more pronounced damage patterns in the samples with time.

3.5 | Bacteriology

The analyzed muscle sample did not show any bacterial or fungal growth.

4 | DISCUSSION

Macroscopically, the mummification status of the human leg did not substantially change over the years. Although certain areas did not yet fully dehydrate, no signs of putrefaction are observable, and the experimentally mummified leg remains in a stable condition.

However, the weight further decreased significantly, which indicates substantial ongoing dehydration. The pH value remained stable with a slightly alkaline value. The surrounding natron salt blend may explain this. As a result of this, the alkaline environment is of significance for molecular analyses since DNA can be better preserved in such a setting. The absence of bacteria and fungi also indicates a stable environment without ongoing putrefaction.

Several years after the end of the first stage of the experiment, DNA degradation is still ongoing, although at a slower pace compared to the first year of mummification. DNA degradation is much more pronounced in muscle tissues in comparison to the skin. Therefore, we observed the DNA in the skin to be more resistant to environmental influences. As we demonstrated in our experiment with artificially mummified pig organs (Öhrström et al., submitted), DNA preservation positively correlates with tissue density. Moreover, the upper layers of the mummified leg dried out quicker during the natron treatment in comparison to the deeper layers, which likely protected DNA in the skin from hydrolysis and oxidation and, as a result, from chemical transformation. Based on the results of our experiment, we recommend considering mummified skin samples as a valuable resource for ancient DNA work since it may yield higher quantity and

better quality DNA in comparison to muscle samples. Since skin is directly exposed to the environment, it should be noted that these tissues often have been contaminated over the years. However, it is essential to remember that work with ancient skin samples requires strict precautions to avoid modern contamination.

All tissues are preserved and identifiable on CT and MRI scans, however further altered in comparison to the initial publication of Panzer et al., mainly showing more tissue-shrinkage and more air inclusions. The appearance now resembles ancient examples of artificially or naturally mummified human remains.

The CT measurements demonstrated an increase in HU in the subcutis, and a decrease in the cutis, cartilage, and compact bone. The increase of HU values in the cutis is a common phenomenon, as reported by other radiological investigations of mummified tissues. A likely explanation is direct contact with the natron salt blend and therefore, a more significant dehydration effect region. Whereas the change of HU was consistent with the trend seen before regarding the cutis and subcutis, the values for cartilage and compact bone instead demonstrate an opposite trend.

Compared to the histological examination at the end of the first phase of the experiment, both muscle and skin show a similar spectrum of microscopic alterations, but there is some evidence of an increased level of decay. In particular, the structure of the epidermis is further altered and partially destroyed, while the subcutis and dermis appear similar in terms of preservation. The muscle tissue can be clearly identified and its anatomical features described, but in comparison, the structure is clearly altered, and no cell nuclei are visible. In some structures, such as the medium-sized vein examined, microscopic features are remarkably well preserved also after 9 years of mummification.

5 | CONCLUSIONS

This follow-up study shows that the experimentally mummified human leg has remained in a mummified condition over several years, and although it did still not completely dehydrate, no decomposition occurred. However, the tissue structure has further altered in the meantime on a molecular, radiological as well as on a histological level, and even several years after the end of the mummification experiment, the process is likely still ongoing. As a result of this, our experimental setup simulates an essential step of artificial as well as certain natural mummification processes, namely dehydration. While we could show that putrefaction was successfully inhibited, the dehydration process did surprisingly not cease, even after several years.

This observance may be explained by the laboratory environment with a relatively high level of humidity. Furthermore, the ancient Egyptians might have periodically exchanged the natron, which was not the case in our experiment. Based on the results of our experiment, mummified skin samples may constitute a valuable resource for ancient DNA since it can yield higher quantity and better quality DNA in comparison to other soft tissue samples, if contamination can be avoided.

ORCID
Lena M. Öhrström https://orcid.org/0000-0003-2192-4520

REFERENCES

Aufderheide, A. C. (2000). Progress in soft tissue paleopathology. *JAMA*, *284*, 2571–2573.

Bergeest, J., & Jäger, F. (2008). A comparison of five methods for signal intensity standardization in MRI. In T. Tolxdorff, J. Braun, T. M. Deserno, A. Horsch, H. Handels, & H. Meinzer (Eds.), *Bildverarbeitung für die Medizin 2008. Informatik aktuell*. Berlin, Heidelberg: Springer.

Brier, B., & Wade, R. (1997). The use of Natron in human mummification: A modern experiment. *Zeitschrift Fur Agyptische Sprache Und Altertumskunde*, *124*, 89–100.

Diodorus, S. (1985). *Diodorus on Egypt (Translated by Edwin Murphy)*. London: McFarland & Company.

Garner, R. (1979). Experimental mummification. In A. R. Dravid (Ed.), *The Manchester Museum mummy project* (pp. 19–24). Manchester: Manchester University Press.

Gilbert, M. T., Hansen, A. J., Willerslev, E., Rudbeck, L., Barnes, I., Lynnerup, N., & Cooper, A. (2003). Characterization of genetic miscoding lesions caused by postmortem damage. *American Journal of Human Genetics*, *72*, 48–61.

Herodot, F. J. (2000). *Historien 1/2. Zweisprachige Ausgabe: Griechisch-Deutsch*. Düsseldorf: Artemis & Winkler.

Hofreiter, M., Jaenicke, V., Serre, D., von Haeseler, A., & Paabo, S. (2001). DNA sequences from multiple amplifications reveal artifacts induced by cytosine deamination in ancient DNA. *Nucleic Acids Research*, *29*, 4793–4799.

Ikram, S., & Dodson, A. (1998). *The mummy in ancient Egypt: Equipping the dead for eternity*. New York: Thames & Hudson.

Kircher, M., Sawyer, S., & Meyer, M. (2012). Double indexing overcomes inaccuracies in multiplex sequencing on the Illumina platform. *Nucleic Acids Research*, *40*, e3.

Meyer, M., & Kircher, M. (2010). Illumina sequencing library preparation for highly multiplexed target capture and sequencing. *Cold Spring Harbor Protocols*, *2010*(6), 1–10.

Notman, D., & Aufderheide, A. (1992). Experimental mummification and computed imaging. In *I world congress on mummy studies* (pp. 821–828). Tenerife, Canary Islands Museo Arquelogico y Etnografico de Tenerife: Organismo Autonomo de Museos y Centros Actas deI Congreso Internacional de Estudios Sobre Momias.

Oh, C. S., & Shin, D. H. (2014). Making an animal model for Korean mummy studies. *Anthropologischer Anzeiger*, *71*, 469–488.

Panzer, S., Borumandi, F., Wanek, J., Papageorgopoulou, C., Shved, N., Colacicco, G., & Rühli, F. J. (2013). Modeling ancient Egyptian embalming: Radiological assessment of experimentally mummified human tissue by CT and MRI. *Skeletal Radiology*, *42*, 1527–1535.

Papageorgopoulou, C., Shved, N., Wanek, J., & Rühli, F. J. (2015). Modeling ancient Egyptian mummification on fresh human tissue: Macroscopic and histological aspects. *Anatomical Record*, *298*, 974–987.

Peltzer, A., Jager, G., Herbig, A., Seitz, A., Kniep, C., Krause, J., & Nieselt, K. (2016). EAGER: Efficient ancient genome reconstruction. *Genome Biology*, *17*, 60.

Shved, N., Haas, C., Papageorgopoulou, C., Akguel, G., Paulsen, K., Bouwman, A., ... Ruhli, F. (2014). Post mortem DNA degradation of human tissue experimentally mummified in salt. *PLoS One*, *9*, e110753.

Thompson, R. C., Allam, A. H., Lombardi, G. P., Wann, L. S., Sutherland, M. L., Sutherland, J. D., ... Thomas, G. S. (2013). Atherosclerosis across 4000 years of human history: The Horus study of four ancient populations. *Lancet*, *381*, 1211–1222.

SUPPORTING INFORMATION

Additional supporting information may be found online in the Supporting Information section at the end of this article.